Effect of donor-acceptor defect pairs on the electrical and optical properties of $CuIn_3Te_5$

2002 J. Phys.: Condens. Matter 14 997

(http://iopscience.iop.org/0953-8984/14/5/305)

INSTITUTE OF PHYSICS PUBLISHING JOURNAL OF PHYSICS: CONDENSED MATTER

J. Phys.: Condens. Matter **14** (2002) 997–1009 PII: S0953-8984(02)29258-9

Effect of donor–acceptor defect pairs on the electrical and optical properties of $CuIn_3Te_5$

C Rincón, S M Wasim and G Marín

Centro de Estudios de Semiconductores, Departamento de Física, Facultad de Ciencias, Universidad de Los Andes, Apartado Postal No 1, La Hechicera, Mérida 5101, Venezuela

Received 28 September 2001, in final form 12 December 2001
Published 25 January 2002
Online at stacks.iop.org/JPhysCM/14/997

Abstract

The electrical and optical properties of the *ordered defect compound* $CuIn_3Te_5$ have been studied. Above around 125 K, the electrical conduction is due to the activation of a shallow acceptor level of about 30 meV. The temperature dependence of the mobility in the high-temperature regime is explained by considering an additional scattering mechanism of the free holes with donor–acceptor defect pairs. At lower temperatures the mobility can be explained by using an expression for a variable-range-hopping conduction mechanism. The analysis of the temperature dependence of the optical data shows that the band-gap energy varies from 1.08 to 1.00 eV between 10 and 300 K. As in other copper ternaries, the phonon energy, much higher than the highest optical phonon mode, associated with the Urbach tail and the temperature dependence of the Urbach energy, is explained on the basis of the contribution of localized modes produced by structural disorders of low formation energy.

1. Introduction

The n-type ternary compound $CuIn_3Se_5$ is found to segregate as a secondary phase on the surface of In-rich $CuInSe_2$ thin films [1]. Since it was suggested that this material could play an important role in the operation and optimization of $CuInSe_2$-based solar cells [2], several works on the physical properties of bulk and thin-film samples of $CuIn_3Se_5$ [3–9] and $CuIn_5Se_8$ [8] have been carried out in the last few years. On the other hand, Zhang *et al* [10,11], in their pioneering works, have explained the existence and stability of these compounds as due to the presence in $CuInSe_2$ of ordered arrays of $(In_{Cu}^{2+} + 2\ V_{Cu}^{-1})$ donor–acceptor defect pairs (DADPs) that have very low formation energies. They have established that $CuIn_5Se_8$, $CuIn_3Se_5$, $Cu_2In_4Se_7$, and $Cu_3In_5Se_9$ originate from a single unit of $(In_{Cu}^{2+} + 2\ V_{Cu}^{-1})$ in each $n = 4$, 5, 7, and 9 units, respectively, of $CuInSe_2$. Because of the presence of DADPs, these compounds are referred to in the literature as *ordered defect compounds* (ODCs). It can thus be considered that these selenides have importance not only in the fabrication of electro-optical

devices but also in understanding the physics and chemistry of ordered arrays of DADPs and how they affect the electrical and optical properties.

The corresponding tellurides of these ODCs, such as $CuIn_3Te_5$, $CuGa_3Te_5$, $CuIn_5Te_8$, and $CuGa_5Te_8$, are also of technological and academic interest and some works on their growth conditions and structural, electrical, and optical parameters at room temperature have been reported recently [8, 12, 13]. However, no detailed study on the temperature dependence of their electrical and optical properties appears in the literature. Hence, in the present article, we report on the analysis of the temperature dependence of the electrical resistivity ρ, hole concentration p, mobility μ, and the optical absorption coefficient α of $CuIn_3Te_5$. To establish the effect of DADP in this compound, these parameters are compared with the data published earlier on the normal $CuInTe_2$ phase, which does not have the ordered arrays of DADPs. The lower value of the hole concentration as compared to the lowest value reported for $CuInTe_2$ is attributed to the fact that DADPs in $CuIn_3Te_5$ are expected to be electrically inactive and do not contribute to the free charge carriers. The temperature dependence of μ in the high-temperature regime is explained by considering an additional scattering mechanism of the free carriers with DADPs. From the analysis of the absorption coefficient α at different temperatures, the variation of the energy band gap E_G with T is established. A study of the Urbach tail, observed just below the band edge, is also made. The relatively high value of the phonon energy associated with the Urbach tail is explained in terms of the localized modes, created by the presence of intrinsic defects, with energy above that of the pure optical band.

2. Experimental details

Ingots of $CuIn_3Te_5$ were prepared by the vertical Bridgman–Stockbarger technique as described elsewhere [12]. The chemical analysis of the samples taken from the central part of the ingots, performed by energy-dispersive x-ray (EDX) spectroscopy, gave a representative composition of Cu:In:Te as 10.44:33.60:55.56 at.% very close to the ideal 1:3:5 value. The error in the standardless analysis was around 5%. This indicates that the homogeneous 135 phase in the Cu–In–Te system, stable at room temperature, is effectively formed. However, there is a slight excess of In with respect to Cu (In/Cu $\approx$ 3.2) and of Te over cations (Te/metal $\approx$ 1.26).

Analysis of powder diffraction x-ray patterns confirms that the compound crystallizes in a tetragonal unit cell corresponding to a chalcopyrite-related structure [12]. The unit-cell parameters a and c thus obtained are 6.1639(3) and 12.346(2) Å, respectively. All the samples showed p-type conductivity, as determined by a thermal probe. The electrical resistivity ρ and carrier concentration p in a magnetic field of 10 kOe were measured on rectangular samples of representative dimensions $(1 \times 2 \times 8)$ mm^3 between liquid nitrogen and room temperature. The optical absorption coefficient α was measured with an automated Cary 17 spectrophotometer; details of this method are given in [4].

3. Results and discussion

3.1. Electrical properties

The variation of p as a function of $1000/T$ is plotted in figure 1. In the same figure we also plot the temperature dependence of p for a sample of $CuInTe_2$ that has the lowest hole concentration reported in the literature at room temperature. This is to establish (to be described later) the existence of DADPs in $CuIn_3Te_5$ and their effect on the magnitude of the majority charge carriers. A comparison of the two curves, where the p versus T data for $CuIn_3Te_5$ fall about two orders of magnitude below those for $CuInTe_2$, is strongly indicative of an electrically

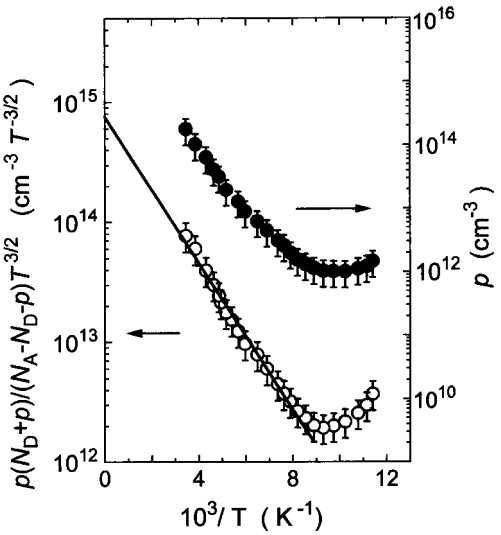

Figure 1. Plots of the hole concentration p (●) (right scale) and $[p(p+N_D)/T^{3/2}(N_A-N_D-p)]$ (○) (left scale), on a logarithmic scale, against $10^3/T$ for $CuIn_3Te_5$. The fit of equation (1) to the data above about 120 K is shown by the continuous curves.

inactive nature of the DADPs. The behaviour of $p(T)$ suggests that above around 130 K, the electrical conduction in $CuIn_3Te_5$ is mainly due to activation in the valence band and below about 120 K, due to the charge carriers in the impurity band. To estimate the activation energy E_A of the acceptor level and the effective mass m_h^* of the hole from the high-temperature data, we use the well-known expression for non-degenerate statistics in the valence band [14]

$$p_v(p_v + N_D)/(N_A - N_D - p_v) = (N_v/g)\exp(-E_A/kT). \tag{1}$$

In this expression p_v is the concentration of holes and $N_v = 2(m_h^* k_B T/2\pi\hbar^2)^{3/2}$ is the effective density of states in the valence band. N_A and N_D are the acceptor and compensating donor concentrations, and g the degeneracy factor of the acceptor ground state. For the analysis of the data in the high-temperature region, it is assumed that the contribution of the impurity band to the total hole concentration p is negligible. Thus, by replacing p_v with the measured value p, a linear plot of $\ln[p(p + N_D)/T^{3/2}(N_A - N_D - p)]$ is obtained against $10^3/T$ with the adjustable parameters $N_A = (5.1 \pm 0.5) \times 10^{17}$ cm^{-3} and $N_D = (5.0 \pm 0.4) \times 10^{17}$ cm^{-3}. This is also shown in figure 1. From the slope, E_A is calculated to be 30 ± 5 meV. Also, assuming $g = 4$, which is the value of the degeneracy factor observed in the case of $CuInTe_2$ where the heavy- and light-hole valence bands are degenerate [15], from the intercept of the straight line at $10^3/T \to 0$, the effective mass m_h^* of the hole in $CuIn_3Te_5$ is estimated to be $(0.73 \pm 0.04)m_e$. This can be compared with $m_h^* \approx 0.78m_e$ reported [16, 17] for $CuInTe_2$, indicating that the structure of the valence band of this compound and that of $CuIn_3Te_5$ are very much similar. This also confirms that $CuIn_3Te_5$ is formed due to the presence of a single unit of $(In_{Cu}^{2+} + 2\,V_{Cu}^{-1})$ in each five units of $CuInTe_2$.

The activation energy of the acceptor level in $CuIn_3Te_5$ is in good agreement with $E_A = 38 \pm 8$ meV, calculated from the expression [18] $E_A(N) = E_{A0} - \beta N^{1/3}$, which takes into account the screening effect of the charge carries by impurities. In this calculation, the activation energy E_{A0} in the dilute limit is estimated by using the hydrogenic model for a single-acceptor level ($E_{A0} \approx 13.6m_h^*/m_e\varepsilon_0^2$) with $\varepsilon_0 \approx 12$ (to be discussed later). For the screening constant we use $\beta = 3 \times 10^{-8}$ eV cm^{-1} which is the value obtained for ternary

chalcopyrites [17]. The impurity concentration N used in the calculation is the total ionized defect concentration, $N_I = N_A + N_D \approx 1.1 \times 10^{18}$ cm^{-3}. This level can be attributed to copper vacancies (V_{Cu}), and is expected to lead to a single-acceptor state in the present case. This identification would be consistent with EDX analysis which indicates that our samples are Cu poor. The other possible origin of this level, since the sample is also Te rich according to EDX analysis, could be the double-acceptor state due to the tellurium interstitial (Te_i). However, this possibility is discarded, because the calculated E_{A0} for the two levels of such a double state [19] is expected to be 1.7 and 4 times higher than that for the single state. This gives, for the two levels of Te_i, $E_A \approx 90$ and 250 meV, respectively, which are considerably higher than those obtained from the electrical data. This result indicates that shallow acceptor levels observed in $CuInTe_2$, that probably originate from copper vacancies, are partially annihilated when $CuIn_3Te_5$ is formed due to the attractive interaction between In_{Cu}^{2+} and V_{Cu}^{-1}. This is consistent with the fact that the concentration of the shallow acceptor levels observed in the present case ($N_A \approx 5 \times 10^{17}$ cm^{-3}) is at least one order of magnitude lower than that obtained in $CuInTe_2$ which varies from 3 to 46×10^{18} cm^{-3} [16, 17]. The fact that the activation energy of the acceptor level due to the copper vacancy in $CuIn_3Te_5$ is higher than the values of E_A for $CuInTe_2$, which lie between 9 and 22 meV [16, 17], can be explained as due to the partial annihilation of these levels due to DADPs and to the screening effect. It has been shown [17] that in the dilute limit of hole and acceptor concentrations, the value of the activation energy of the shallow acceptor level in $CuInTe_2$ is $E_{A0} \approx 30$ meV that is in excellent agreement with that obtained for $CuIn_3Te_5$.

The logarithmic variation of ρ with $1000/T$ is plotted in figure 2 (lower scale). From the temperature-dependent behaviour of the hole concentration in figure 1, it is inferred that the electrical conduction below about 120 K is predominantly due to charge carriers in the impurity band. In the absence of a linear dependence in this plot in this temperature range that would indicate a nearest-neighbour hopping conduction, $\ln \rho$ was plotted as a function of $100/T^{1/4}$ and $100/T^{1/2}$. The best fit, although in the limited temperature range between 80 and 125 K, was obtained with the latter. This is also shown in figure 2 (upper scale). This suggests that the conduction in the impurity band is due to a variable-range-hopping mechanism of Efros–Shklovskii type [20] with $\rho = \rho_{0ES} \exp(T_{0ES}/T)^{1/2}$. The parameters obtained from the fit are $\rho_{0ES} \approx 1.4 \times 10^3\ \Omega$, and $T_{0ES} \approx 2.2 \times 10^3$ K. This value of T_{0ES} is of the same order as that reported for $CuInTe_2$, which is 3.4×10^3 K [21].

The variation of the hole mobility μ with temperature for $CuIn_3Te_5$ is shown in figure 3. Its magnitude at 300 K is also very nearly two orders of magnitude smaller in comparison to that observed for $CuInTe_2$, which varies from 27 to 135 cm^2 V^{-1} s^{-1} [16]. The strengths of the different scattering mechanisms responsible for the hole mobility μ_v at temperatures above 125 K, which is the temperature region where electrical transport due to holes in the valence band is dominant, were calculated by using the Mathiessen rule

$$\mu_v^{-1} = \mu_I^{-1} + \mu_{AC}^{-1} + \mu_{PO}^{-1} + \mu_{NPO}^{-1} + \mu_N^{-1} \tag{2}$$

where μ_I, μ_{AC}, μ_{PO}, μ_{NPO}, and μ_N represent the mobilities of holes due to the scattering by ionized impurities, acoustic, polar, and non-polar optical modes, and neutral impurities, respectively.

The Hall mobility due to ionized impurity scattering is calculated according to the Brooks–Herring formula [22–24]:

$$\mu_I = (2/300) 2^{7/2} \varepsilon_0^2 (k_B T)^{3/2} \pi^{3/2} e^3 (m_h^*) N_I f(x). \tag{3}$$

Here ε_0 is the static dielectric constant, N_I the ionized impurity concentration, and the function $f(x)$ is given by the relation $\ln(1+x) - x/(1+x)$, where $x = 6\varepsilon_0 m_h^* (k_B T)^2 \pi e^2 h^2 p$.

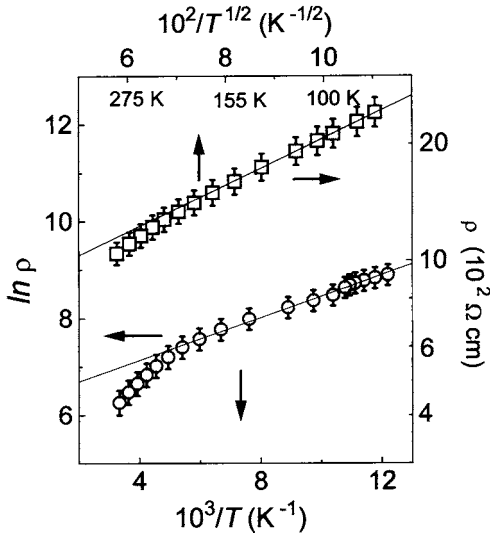

Figure 2. Plots of the logarithmic variation of electrical resistivity ρ against $10^3/T$ (○) (right and lower scales) and ln ρ against $10^2/T^{1/2}$ (□) (left and upper scales), for $CuIn_3Te_5$. The nearly linear behaviour of ln ρ versus $10^2/T^{1/2}$, between 80 and 125 K, is shown by the continuous curve.

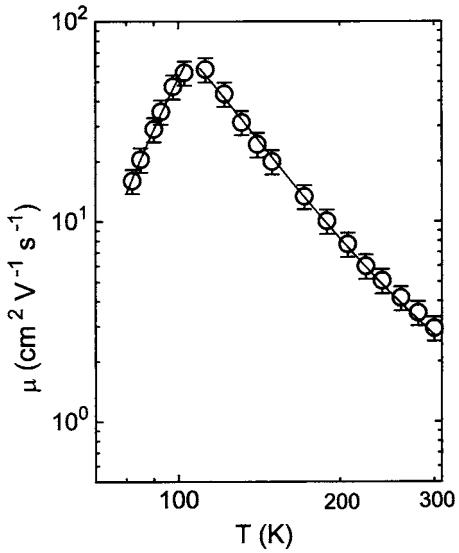

Figure 3. Variation of hole mobility μ with temperature on a logarithmic scale for $CuIn_3Te_5$ (○). The continuous curves represent the theoretical fit to the data in the activation and hopping conduction regimes with the scattering mechanisms mentioned in the text.

The acoustic mode scattering mobility is given by [23, 24]

$$\mu_{AC} = (2/300)(8\pi)^{1/2} e\rho\hbar^4 v^2 / 3E_{AC}^2 (m_h)^{*5/2} (k_B T)^{3/2} \tag{4}$$

where E_{AC} is the valence band deformation potential. The mass density $\rho = 5.23$ g cm^{-3} and the longitudinal velocity of sound $v \approx 2 \times 10^5$ cm s^{-1}, used in the calculation, were estimated from the x-ray diffraction data and the Debye temperature $\theta_D \approx 168$ K (to be discussed later), respectively.

For the polar optical phonon mobility, the expression used is [23, 24]

$$\mu_{\mathrm{PO}} = 25.4(T^{1/2}/m_{\mathrm{h}}^{*3/2}\theta)(1/\varepsilon_\alpha - 1/\varepsilon_0)^{-1}[\exp(\theta/T) - 1]G(\theta/T) \tag{5}$$

where ε_α is the high-frequency dielectric constant and $G(\theta/T)$ is a tabulated function which may be approximated, in the range from 100 to 300 K, by $0.48\exp(0.18\theta/T)$.

The non-polar optical phonon mobility is calculated from the expression to first order in the phonon wavevector [25]

$$\mu_{\mathrm{NPO}} = \pi^{1/2}e\rho\hbar^4[18^{1/2}D_{\mathrm{I}}^2 m_{\mathrm{h}}^{*7/2}(k_{\mathrm{B}}\theta_\alpha)^2(k_{\mathrm{B}}T)^{5/2}]^{-1} \tag{6}$$

where D_{I} represents the first-order coupling constant and θ_α a characteristic phonon temperature.

The contribution of the neutral impurity scattering to the Hall mobility has been calculated by using the Erginsoy formula [24, 26]

$$\mu_{\mathrm{N}} = (2/300)e^3 m_{\mathrm{h}}^{*1/2}/20\varepsilon_0\hbar^3 N_{\mathrm{N}} \tag{7}$$

where N_{N} is the neutral impurity concentration.

An attempt was made to fit equation (2) with the mobility data above 125 K where the conduction is due to activation mechanism. However, this was not possible with reasonably acceptable values of the adjustable parameters involved in equations (3)–(7). This suggests the possibility of an additional scattering mechanism of the holes, most probably with DADPs.

To estimate the strength of this scattering mechanism in $CuIn_3Te_5$ and to fit the experimental data of μ versus T using the Mathiessen rule in the activation regime, it is assumed, in a first approximation, that this scattering can be treated as a simple collision problem. Then, at a given temperature, the probability per unit time $1/\tau_{\mathrm{DAP}}$ for the collision of holes with DADP should be proportional to the product of the concentrations of free holes p_{v} and defect pairs N_{DP}. These concentrations can be approximated by $p_{\mathrm{v}}(T) \approx A(T)\exp(-E_{\mathrm{A}}/k_{\mathrm{B}}T)$ and $N_{\mathrm{DP}}(T) \approx N_{\mathrm{a}}B(T)\exp(-H/k_{\mathrm{B}}T)$, respectively. In these relations $A(T)$ and $B(T)$ are expected to be slowly varying functions of T and can be considered as constants, N_{a} are the concentrations of atoms in the crystal, and H is the formation energy of the arrays of defect pairs. Thus, the contribution to μ in the valence band due to the scattering of holes by DADP can be expressed by

$$\mu_{\mathrm{DP}} \approx e\tau_{\mathrm{DAP}}/m_{\mathrm{h}}^* \approx \mu_0\exp[(E_{\mathrm{A}} + H)/k_{\mathrm{B}}T] \tag{8}$$

where μ_0, a nearly constant parameter, depends mainly on N_{a} and m_{h}^*. The temperature dependence of μ in figure 3 above 125 K, in the activation regime, was fitted by taking into account the combined effect of the scattering of the charge carriers by DADP, ionized impurities, and acoustic and non-polar optical phonons. Optical phonons were not included in the final fit because, as reported [24], they are not expected to contribute to the scattering of carriers in p-type samples of the chalcopyrite compounds. Also, neutral impurities were not taken into account because the impurity level detected from the electrical measurement is very shallow ($E_{\mathrm{A}} \approx 30$ meV). Hence, such a mechanism is expected to contribute to the hole mobility only at very low temperatures ($T < 80$ K).

In the fit, the static dielectric constant ε_0, the optical constant ε_α, the deformation potential E_{AC} of the p-type valence band, H, μ_0, and D_{I} were considered as adjustable parameters. Others, like the ionized impurity concentration $N_{\mathrm{I}} = N_{\mathrm{A}} + N_{\mathrm{D}}$, m_{h}^*, and E_{A}, were those obtained from the analysis of the carrier concentration data. θ_α was assumed to be equal to 130 K, obtained from the fit of E_{G} versus T data (to be discussed latter), and $\varepsilon_0/\varepsilon_\alpha$ was taken as 1.7, which is the average obtained for Cu ternaries [24]. An excellent fit, as shown in figure 3 by continuous curve, is obtained with the values of $\varepsilon_0 = 12 \pm 2$, $E_{\mathrm{AC}} = 6.2 \pm 1.5$ eV, $H = 32 \pm 4$ meV, $\mu_0 \approx 0.3\ \mathrm{cm^2\ V^{-1}\ s^{-1}}$, and $D_{\mathrm{I}} \approx 200$ eV. Values of ε_0 and E_{AC} are nearly of

the same magnitude as those reported for $CuInTe_2$ which are about 10 and 5 eV, respectively. Although no calculations of the formation energy of ordered DADP arrays in $CuInTe_2$ have been reported, $H \approx 30$ meV is in good agreement with that calculated for $CuInSe_2$ which is around 10 meV [10].

At low temperatures, where a variable-range-hopping conduction mechanism of the Efros–Shklovskii type is predominant, the expression [27] $\mu_I = \mu_0 \exp(-T_0/T)^s$ is used to fit the mobility data. The values of μ_0, T_0, and s thus obtained are 1.3×10^4 cm^2 V^{-1} s^{-1}, 1.02×10^3 K, and 0.50, respectively. $T_0 \approx 1.02 \times 10^3$ K is comparable to $T_{0ES} \approx 2.2 \times 10^3$ K obtained from the analysis of ρ versus T data. An estimate of the localization length ξ, involved in the variable-range-hopping conduction, is made through the relation [20]

$$\varepsilon_0 \xi \approx 2.8e^2/k_B T_{0ES}. \tag{9}$$

With the values of T_{0ES} obtained from resistivity and mobility data, $\varepsilon_0\xi$ for $CuIn_3Te_5$ is estimated to be 200 and 460 Å, respectively. These values are physically more reasonable than those reported for n-type CdSe [28] which are quite high, of the order of 10^4 Å.

3.2. Absorption coefficient spectra

The absorption coefficient α can be calculated from the measured transmittance T through the relation $\alpha(h\nu) = (1/t)[2\ln(1-R) - \ln T]$, where R is the reflectivity and t the thickness of the sample. To determine the value of E_G, the absorption coefficient spectra of $CuIn_3Te_5$ at different temperatures, shown in figure 4, were analysed using an expression obtained from the Elliot model [29] after convoluting the total absorption coefficient with a Lorentzian function, $\Gamma\pi^{-1}[(h\nu)^2 + \Gamma^2]$. According to this approach, α can be expressed by [4]

$$\alpha = \alpha_0 \sum_n (1/n^3)(\Gamma_n/2)^2/[(\Gamma_n/2)^2 + (h\nu - E_G + R_X/n)^2] + \alpha_1\{\pi/2 + \arctan[(h\nu - E_G)\Gamma_c/2)]\} \tag{10}$$

where α_0 and α_1 represent the absorption peak at the ground-state exciton energy and the absorption at the energy gap, respectively. Γ_n and Γ_c are the full width at half-maximum of the Lorentzian and the full width of the continuum excitons, respectively, and R_X the free-exciton binding energy. In the fit, only the $n = 1$ term was included in the summation. Higher values of n were neglected due to the n^{-3}-dependence of the peak intensity of free excitons. The theoretical absorption curves thus obtained, with the data shown in table 1, are also shown in figure 4 by continuous curves. The temperature dependence of the energy gap of a representative sample of $CuIn_3Te_5$ is shown in figure 5. E_G versus T data for $CuInTe_2$ sample S-690, obtained in [30], are also plotted for comparison.

It can be observed from figure 5 that the value of E_G for $CuIn_3Te_5$ at each temperature is roughly 20 meV higher than that for $CuInTe_2$. This is different from what has been reported for $CuIn_3Se_5$ and $CuGa_3Se_5$, where E_G is higher than in its corresponding 1:1:2 phase by about 0.2 eV [11, 31]. According to the calculation carried out by Zhang *et al* [11], Cu–In–Se ODCs are formed due to the low formation energy and the high stability of the $(2\,V_{Cu}^{1-} + In_{Cu}^{2+})$ defect pair. The creation of periodic V_{Cu}, in the case of $CuIn_3Se_5$ unlike in that of $CuInSe_2$, causes a reduction of the Se p–Cu d interband repulsion due to the decrease of the degree of d character. This leads to the lowering of the valence band maxima (VBM) of $CuIn_3Se_5$. Although the presence of a repeated $(2\,V_{Cu}^{-1} + In_{Cu}^{+2})$ pair in $CuIn_3Se_5$ also lowers the conduction band minimum (CBM), the lowering of the VBM is greater in this system because of the initially very strong p–d repulsion in $CuInSe_2$. Thus, the band gap of $CuIn_3Se_5$ is larger than that of $CuInSe_2$. On the other hand, the d character of $CuInTe_2$ is much weaker as compared to that of $CuInSe_2$ [8]. Since the band gaps of $CuIn_3Te_5$ and $CuInTe_2$ are very

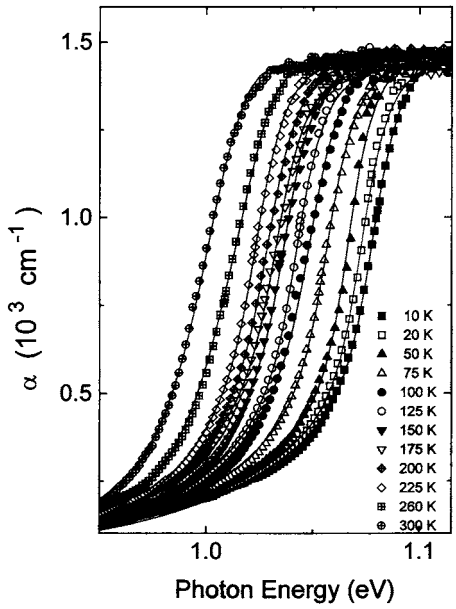

Figure 4. The absorption coefficient α of $CuIn_3Te_5$ at various temperatures between 10 and 300 K. The continuous curves represent the fit of equation (10) to the data with the parameters given in table 1.

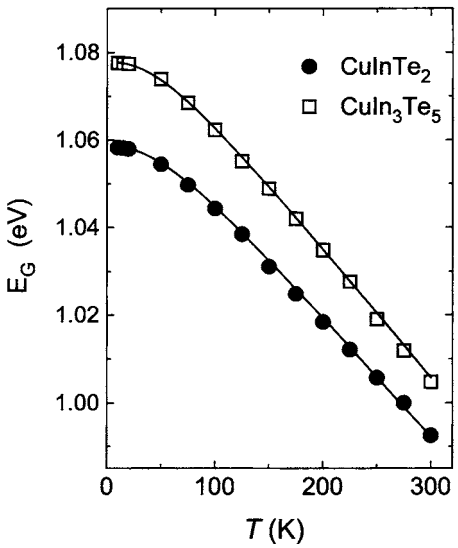

Figure 5. Variation of the energy gap E_G with temperature in $CuIn_3Te_5$ (□) and $CuInTe_2$ (●). Continuous curves represent the theoretical fit of equation (12) to the E_G versus T data with the parameters given in table 2.

nearly the same, one might suggest that the lowering of the CBM in $CuIn_3Te_5$ is very nearly of the same magnitude as that of the VBM. However, a detailed theoretical study, similar to that reported for the Cu–In–Se system, is required for the Cu–In–Te system to confirm this interpretation.

Table 1. Values of the adjustable parameters α_0, α_1, Γ_1, Γ_c, $E_G(0)$, and R_X for $CuIn_3Te_5$ obtained by fitting equation (10) to the optical absorption data at different temperatures between 10 and 300 K shown in figure 4. The possible errors in these parameters are given in parentheses.

T (K)	α_0 (cm^{-1})	α_1 (cm^{-1})	Γ_1 (meV)	Γ_1 (meV)	$E_G(0)$ (meV)	R_X (meV)
10	435(20)	520(18)	81(12)	23(2)	1078(3)	7(2)
20	428(20)	514(20)	80(12)	22(2)	1077(3)	7(2)
50	432(20)	509(23)	75(11)	21(2)	1074(3)	7(2)
75	431(18)	520(19)	78(12)	23(2)	1069(4)	8(2)
100	436(19)	485(18)	83(12)	25(3)	1062(3)	7(3)
125	429(18)	490(20)	84(13)	23(2)	1055(4)	6(3)
150	410(20)	478(20)	76(13)	24(2)	1049(3)	7(2)
175	407(18)	482(18)	80(12)	26(2)	1042(4)	7(2)
200	404(20)	476(20)	82(13)	26(3)	1035(3)	7(2)
225	400(17)	483(18)	85(12)	25(2)	1028(3)	7(3)
260	396(20)	480(18)	78(12)	27(3)	1016(4)	7(2)
300	391(20)	481(20)	85(13)	28(2)	1005(3)	7(2)

Recently, Pässler [32] has proposed an analytical description of E_G versus T within the regime of the dominance of the electron–phonon interaction. According to this theory, this variation can be given by integrals of the form

$$E_G(T) = E_G(0) - \int f(\varepsilon)\bar{n}(\varepsilon, T)\,\mathrm{d}\varepsilon \tag{11}$$

where ε is the phonon energy, $\bar{n}(\varepsilon, T) = [\exp(\varepsilon/k_BT) - 1]^{-1}$ represents the average phonon occupation number, $f(\varepsilon)$ is the relevant electron–phonon spectral function, given in the energy range from 0 to a cut-off value $\varepsilon_{co} = [(\eta + 1)/\eta]k_B\theta$ by a power-law dependence of the form $f(\varepsilon) \propto \varepsilon^{\eta}$. $\varepsilon_{eff} = k_B\theta$ is the effective phonon energy where θ, the effective phonon temperature, is expected to be roughly three quarters of the Debye temperature θ_D.

For exponents within a range $1.2 < \eta < 1.8$, which corresponds to moderately concave spectral functions, equation (11) takes the form [32]

$$E_G(T) = E_G(0) - \delta\theta/2\{[1 + (2T/\theta)^p]^{1/p} - 1\}^{1/2} \tag{12}$$

where δ is equal to the high-temperature limit, $S(\infty)$, of the associated entropy, $S(T) \equiv \mathrm{d}E_G(T)/\mathrm{d}T$, and the parameter $p = \eta + 1$. The exponent η governs the shape of the spectral function.

Equation (12) was fitted to the $E_G(T)$ data of figure 5. Values of the parameters $E_G(0)$, δ, θ, p, ε_{co}, and ε_{eff} obtained from the fit for the $CuInTe_2$ and $CuIn_3Te_5$ samples are given in table 2. The theoretical curve for this equation is also shown in the same figure, as the continuous curve. It is observed that the values of $E_G(0)$ and θ for $CuIn_3Te_5$ are nearly the same as those for $CuInTe_2$. From the values of θ for $CuInTe_2$ and $CuIn_3Te_5$ obtained from the fit, the Debye temperature for these compounds was estimated to be around 180 and 168 K, respectively. θ_D for $CuInTe_2$ is in very good agreement with that obtained from specific heat data, which is 185 K [33]. On the other hand, from Raman spectra at room temperature [13], 16 optical phonon modes have been reported in $CuIn_3Te_5$. The frequency of these modes varies from the lowest at 49 cm^{-1} (~7 meV) to the highest value at 220 cm^{-1} (~27 meV). It is observed that the cut-off energy, $\varepsilon_{co} \approx 19$ meV, obtained from the Pässler model for $CuIn_3Te_5$, is considerably lower than that of the highest-frequency mode at 27 meV. In the absence of the reported frequency of the acoustic phonon modes, only the mean frequency of the optical modes in $CuIn_3Te_5$ could be roughly estimated by considering the modes observed from Raman measurements. The relation used is $\bar{\nu} \approx \sum I_i\nu_i / \sum I_i$, where ν_i and I_i are

Table 2. Values of the adjustable parameters $E_G(0)$, p, δ, and θ, obtained by fitting equation (12) to the $E_G(T)$ data for $CuIn_3Te_5$ and $CuInTe_2$ shown in figure 5. Effective values of the phonon energy ε_{eff} and cut-off ε_{co} for these compounds are also given.

	$E_G(0)$ (eV)	p	δ (10^{-4} eV K^{-1})	θ (K)	ε_{eff} (meV)	ε_{co} (meV)
$CuIn_3T_5$	1.0779 ± 0.0003	2.3 ± 0.1	3.0 ± 0.1	126 ± 11	11 ± 1	19 ± 2
$CuInTe_2$	1.0587 ± 0.0003	2.2 ± 0.1	2.8 ± 0.2	135 ± 10	12 ± 1	21 ± 2

the frequency and the relative intensity of the ith Raman mode, respectively. This gives $\bar{\nu} \approx 127$ cm^{-1} ($\sim$16 meV) which is slightly higher than the effective energy, $\varepsilon_{eff} \approx 11$ meV, of phonons that participate in the temperature variation of the energy gap in $CuIn_3Te_5$. This strongly suggests that in this ODC both acoustic and optical modes participate in the shift of E_G versus T.

3.3. Urbach tail

The logarithmic variation of α with $h\nu$, just below E_G, at several temperatures between 50 and 300 K is plotted in figure 6 from the α versus $h\nu$ data for the same $CuIn_3Te_5$ sample plotted in figure 4. To maintain the clarity of the figure, $\ln\alpha$ versus $h\nu$ is given for a limited number of temperatures. The data points over a reasonably wide range of photon energy in this plot at each temperature can be approximated by a straight line. The extrapolations of these lines tend to converge to a single point defined by α_0 and E_0. This behaviour of the absorption coefficient is in agreement with the Urbach rule [34]. This is expressed by an exponential relation of the form

$$\alpha(h\nu) = \alpha_0 \exp[\sigma(h\nu - E_0)/k_B T] \tag{13}$$

where α_0 and E_0 are characteristic parameters of the material, σ is the steepness parameter, and $k_B T/\sigma$, which represents the width of the exponential tail, is called the Urbach energy E_U. The fit of equation (13) to the absorption data near the band edge, shown in figure 6 by continuous curves that converge to a single point, gives $E_0 \approx 1.28$ eV and $\alpha_0 = 1.85 \times 10^6$ cm^{-1}. E_0, slightly higher than E_G, and the magnitude of α_0 agree quite well with the values reported for other Cu ternaries of the 1:1:2 [35,36] and 1:3:5 phases [6,37].

From the slope of the fitted straight lines in figure 6, σ is calculated at different temperatures. This is plotted in figure 7 as a function of temperature. Using the constant σ_0 and the energy $h\nu_p$ of the phonons associated with the Urbach tail as adjustable parameters, the variation of σ with T is fitted to the empirical relation [38]

$$\sigma = \sigma_0(2k_B T/h\nu_p)\tanh(h\nu_p/k_B T). \tag{14}$$

This fit yields $\sigma_0 = 1.01 \pm 0.03$ and $h\nu_p = 63 \pm 3$ meV. This value of $h\nu_p$ is more than double that of the highest optical phonon mode observed in $CuIn_3Te_5$ which, according to the Raman spectra [13], is at around 27 meV. A similarly large value of $h\nu_p$ is also observed for *normal* 1:1:2 chalcopyrites [35,36] and 1:3:5 ODC [6,37] phases. For example, for $CuIn_3Se_5$, values of $h\nu_p$ in the energy range from 58 to 68 meV were found [6], which are higher than the energy of its highest reported optical mode which is 29 meV [7]. Also similar is the case for $CuGa_3Se_5$, where $h\nu_p$ is 60 meV [37], almost double that for the highest reported mode, around 36 meV [7]. These results indicate that it is not only the optical modes that are involved in the electron–phonon interaction just below the band edge. It has been suggested [6,37] that large $h\nu_p$ could be due to enhanced electronic distortion originating from the ordered defects and structural disorder caused by compositional deviation from ideal stoichiometry. As pointed out by Zhang *et al* [10, 11], due to such deviations, some intrinsic defects, including donor–acceptor defect pairs, are created at low energy cost. Since such defects lower the mass at

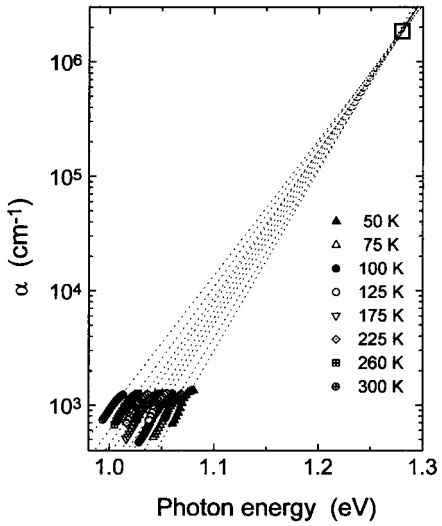

Figure 6. The logarithmic variation of the absorption coefficient spectra at several temperatures between 10 and 300 K, just below E_G, in $CuIn_3Te_5$. The fit of equation (13) to the optical absorption data, shown by continuous curves that converge to a single point, gives $E_0 \approx 1.28$ eV and $\alpha_0 \approx 1.85 \times 10^6$ cm^{-1}.

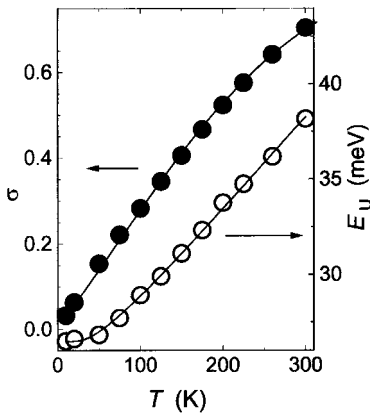

Figure 7. The temperature variation of the steepness parameter σ (●) (left scale) and the Urbach energy E_U (○) (right scale) in $CuIn_3Te_5$. The continuous and dashed curves represent the best fits of equations (14) and (15) to the σ versus T and E_U versus T data, respectively, with the adjustable parameters $\sigma_0 \approx 1.01$ and $h\nu_p \approx 63$ meV from equation (14), and $P \approx 3.80$ and $N \approx 0.58$ from equation (15).

the sites of otherwise unchanged ideal structures, localized modes with energy above the pure optical band can be created [39]. This will be reflected as an increase in $h\nu_p$ associated with the Urbach tail.

The variation of E_U with T for $CuIn_3Te_5$, also shown in figure 7, was compared with the model of Cody *et al* [40] for amorphous semiconductors, which uses a temperature-independent structural disorder parameter X. The best fit, not shown here, but similar to those of [6,35,37], was far from satisfactory. This disagreement is not unexpected, since the physical nature of disorder in amorphous semiconductors should be quite different from the structural defects produced by cation–cation disorder and the deviation from ideal stoichiometry.

To explain the variation of E_U with T, a modified version of the Cody expression [6, 37] is employed that takes the form

$$E_U(T, N, P) = (k_B\theta/\sigma_0)[(1 + P)/2 + N\{\exp(\theta/T) - 1\}^{-1}] \quad (15)$$

where P and N are adjustable parameters related to structural disorder and modification of the thermal phonon distribution, respectively. The first term in this expression, which is independent of temperature, is similar to the structural disorder term proposed by Cody *et al* [40]. The second modifies the thermal term through N which is introduced to take into account the fact that, due to ordered defects and structural disorder, only a fraction of the total phonon modes excited at a given temperature can interact with excitons or electrons [41, 42]. With this relation, E_U versus T data for $CuIn_3Te_5$ are fitted with P and N as adjustable parameters. In the calculation, σ_0 is taken as 1.01, estimated earlier, and $\theta \approx 130$ K obtained from the theoretical fit to the temperature dependence of E_G using equation (12). An excellent fit, also shown in figure 7 by a continuous curve, is obtained with $P = 3.80 \pm 0.4$ and $N = 0.58 \pm 0.01$. Both of these values are in good agreement with those reported for $CuIn_3Se_5$ that vary from 1.96 to 2.53 and 0.37 to 0.47, respectively [6].

4. Conclusions

In summary, the basic electrical and optical properties of p-type $CuIn_3Te_5$ are studied. It is found that at temperatures above around 125 K, the electrical conduction is due to the thermal activation of a shallow acceptor level at around 30 meV due to copper vacancies. Its relatively low hole concentration can be explained as due to the partial annihilation of the shallow acceptor levels originating from copper vacancies in the electrically inactive $(In_{Cu}^{2+} + 2V_{Cu}^{-1})$ donor–acceptor defect pairs. To explain the temperature dependence of its relatively low charge-carrier mobility, a scattering mechanism of the free holes with donor–acceptor defect pairs is proposed. The expression for the mobility related to this new scattering mechanism, calculated from simple first principles, when combined with other well-established mechanisms, explains very well the variation of μ with T in the high-temperature activation regime. At low temperatures, the expression proposed for the mobility in the variable-range-hopping mechanism of Efros–Shklovskii type can be used. From the values of the localization temperature, a physically acceptable value of the localization length is obtained.

In contrast to what has been observed for $CuIn_3Se_5$ and $CuGa_3Se_5$, E_G in the case of $CuIn_3Te_5$ is not very different from that of the corresponding 1:1:2 phase. This can be attributed to the fact that the lowering of the VBM in this ODC, due to the reduction of the degree of d character caused by the incorporation of V_{Cu}, is very nearly of the same magnitude as the lowering of the conduction band minimum originating from the formation of $(In_{Cu}^{+2} + 2\ V_{Cu}^{-1})$ defect pairs.

The optical absorption coefficient spectra near the fundamental edge at different temperatures can be successfully explained by the Elliot model. The $E_G(T)$ dependence thus obtained is explained with the Pässler model. Parameters obtained from the fit allow us to estimate the effective energy of phonon modes that participate in the shift of E_G with T. The value of the phonon energy associated with the Urbach tail is found to be higher than that of the highest optical phonon mode. This is attributed as due to deviations from ideal stoichiometry, cation–cation antisite and other ordered defects that lower the mass at the sites of otherwise unchanged ideal structures and create localized modes above the pure optical band. An empirical relation proposed earlier [6], that takes these effects into account, explains very well the variation of the Urbach energy with temperature.

Acknowledgments

This work was supported by grants from CONICIT (contract No G-97000670), and CDCHT-ULA (contract Nos C-917-98-05-A and C-917-98-05-E).

References

[1] Tiwari A N, Blunier S, Filzmoser M, Zogg H, Schmid D and Schock H W 1994 *Appl. Phys. Lett.* **65** 3347
[2] Yang L C, Xiao H Z, Rockett A, Shafarman W N and Birkmire R W 1995 *Solar Energy Mater. Solar Cells* **36** 445
[3] Nelson A J, Horner G S, Sinha K and Bode M 1994 *Appl. Phys. Lett.* **64** 3600
[4] Marín G, Wasim S M, Rincón C, Sánchez Pérez G, Power C and Mora A E 1998 *J. Appl. Phys.* **83** 3364
[5] Wasim S M, Marín G, Rincón C, Bocaranda P, Masón C, Sánchez Pérez G, Mora A E, Iqbal M and Bacquet G 1998 *Ternary and Multinary Compounds (Inst. Phys. Conf. Ser. 152)* (Bristol: Institute of Physics Publishing) p 55
[6] Wasim S M, Marín G, Rincón C and Sánchez Pérez G 1998 *J. Appl. Phys.* **84** 5823
[7] Rincón C, Wasim S M, Marín G, Delgado J M, Huntzinger J R, Zwick A and Galibert J 1998 *Appl. Phys. Lett.* **73** 441
[8] Wasim S M, Rincón C, Marín G and Delgado J M 2000 *Appl. Phys. Lett.* **77** 94
[9] Rincón C, Wasim S M, Marín G, Rincón A, Bocaranda P, Torres C, Bacquet G and Sánchez Pérez G 1999 *Mater. Lett.* **41** 222
[10] Zhang S B, Wei S H and Zunger A 1997 *Phys. Rev. Lett.* **78** 4059
[11] Zhang S B, Wei S H, Zunger A and Katayama-Yoshida H 1998 *Phys. Rev.* B **57** 9642
[12] Marín G, Delgado J M, Wasim S M, Rincón C, Sánchez Pérez G, Mora A E, Bocaranda P and Henao J A 2000 *J. Appl. Phys.* **87** 7814
[13] Rincón C, Wasim S M, Marín G, Hernández E, Delgado J M and Galibert J 2000 *J. Appl. Phys.* **88** 3439
[14] Blakemore J S 1962 *Semiconductor Statistics* (Oxford: Pergamon) pp 120–52
[15] Thwaites M J, Tomlinson R D and Hampshire M J 1977 *Ternary Compounds 1977 (Inst. Phys. Conf. Ser. 35)* (Bristol: Institute of Physics Publishing) p 237
[16] Wasim S M and Albornoz J G 1988 *Phys. Status Solidi* a **110** 575
[17] Marín G, Wasim S M, Sánchez Pérez G, Bocaranda P and Mora A E 1998 *J. Electron. Mater.* **27** 1351
[18] Monecke J, Siegel W, Ziegler E and Kühnel G 1981 *Phys. Status Solidi* b **103** 269
[19] Rincón C and Márquez R 1999 *J. Phys. Chem. Solids* **60** 1865
[20] Shklovskii B I and Efros A L 1984 *Electronic Properties of Doped Semiconductors* (Berlin: Springer)
[21] Iqbal M, Galibert J, Wasim S M, Hernández E, Bocaranda P and Leotin J 2000 *Phys. Status Solidi* b **219** 351
[22] Brooks H 1955 *Adv. Electron. Electron Phys.* **7** 85
[23] Look D C and Manthuruthil J C 1976 *J. Phys. Chem Solids* **37** 173
[24] Wasim S M 1986 *Solar Cells* **16** 289
[25] Siegel W, Heinrich A and Ziegler E 1976 *Phys. Status Solidi* a **35** 269
[26] Erginsoy C 1950 *Phys. Rev.* **79** 1013
[27] Schön J H, Arushanov E, Fabre N and Bucher E 2000 *Solar Energy Matter.* **61** 417
[28] Zhang Y, Dai P, Levy M and Sarachik M P 1990 *Phys. Rev. Lett.* **64** 2687
[29] Elliot R J 1957 *Phys. Rev.* **108** 1384
[30] Marín G, Rincón C, Wasim S M, Power Ch, and Sánchez Pérez G 1997 *J. Appl. Phys.* **81** 7580
[31] Wei S H, Zhang S B and Zunger A 1998 *Appl. Phys. Lett.* **72** 3199
[32] Pässler R 1996 *Phys. Status Solidi* b **193** 135
[33] Bohmammel K, Deus P, Kühn G and Möller W 1982 *Phys. Status Solidi* a **71** 505
[34] Urbach F 1953 *Phys. Rev.* **92** 1324
[35] Shioda T, Chichibu S, Irie T and Nakanishi H 1996 *J. Appl. Phys.* **80** 1106
[36] Wasim S M, Marín G, Rincón C and Sánchez Pérez G and Mora A E 1998 *J. Appl. Phys.* **83** 3318
[37] Wasim S M, Marín G, Rincón C, Bocaranda P, and Sánchez Pérez G 2000 *J. Phys. Chem. Solids* **61** 669
[38] Kurik M V 1971 *Phys. Status Solidi* a **8** 9
[39] Dean P 1972 *Rev. Mod. Phys.* **44** 127
[40] Cody G D, Tiedje T, Abeles B and Goldstein Y 1981 *Phys. Rev. Lett.* **47** 1480
[41] Wasim S M, Rincón C, Marín G, Bocaranda P, Hernández E, Bonalde I and Medina E 2001 *Phys. Rev.* B **64** 195101
[42] Rincón C, Wasim S M, Marín G, Márquez R, Nieves L, Sánchez Pérez G and Medina E 2001 *J. Appl. Phys.* **90** 4423